Polymer Bulletin (2022) 79:10881–10908
https://doi.org/10.1007/s00289-021-04071-4

ORIGINAL PAPER

Evaluation of physicochemical properties of polycaprolactone/gelatin/polydimethylsiloxane hybrid nanofibers as potential scaffolds for elastic tissue engineering

Mahdieh Dehghan[1,2] · Habib Nikukar[2,3] · Mohammad Khajeh Mehrizi[1]

Received: 1 March 2021 / Revised: 23 December 2021 / Accepted: 27 December 2021 /
Published online: 11 January 2022

Abstract

Hybrid polymers have been used as biomaterials for tissue engineering recently. In this study, the hybrid fibrous scaffolds of polycaprolactone (PCL), gelatin (G) and polydimethylsiloxane (PDMS) with two various types of fiber arrangement were fabricated with different mass ratio by electrospinning. Physicochemical properties of fabricated scaffolds were evaluated using scanning electron microscopy, the immersion of scaffold samples, attenuated total reflectance Fourier transform infrared, X-ray diffraction and tensile strength analysis. Cytotoxicity analyses of scaffolds and human foreskin fibroblasts on the scaffolds were assessed by 3-(4, 5-dimethylthiazoyl-2-yl) 2, 5-diphenyltetrazolium bromide assay. Attachment to the scaffolds and morphology of fibroblasts on them were evaluated by hematoxylin–eosin staining and scanning electron microscopy. Networks and nanofibers less than 30 nm were created throughout the normal nanofibers of PCL/G/PDMS hybrid scaffolds that the efficiency of the homing and proliferation of the fibroblasts cells onto the scaffolds was improved. The PCL/G/PDMS hybrid scaffolds characteristics, especially morphology, mechanical properties and biocompatibility by altering the ratio PCL, G and PDMS show that these scaffolds are suitable for random and aligned tissue engineering applications, especially engineering of elastic tissues (nerve, uterus, bladder, trachea, heart valves, vein, vagina, liver, skin and others).

Keywords Elastic tissue engineering · Hybrid nanofibers · Physicochemical properties · Scaffolds · Polymers

✉ Mohammad Khajeh Mehrizi
mkhajeh@yazd.ac.ir

Extended author information available on the last page of the article

Introduction

Tissue engineering strategies are founded on pathologic tissue regeneration with supportive scaffolds and biological molecules and cells. Biologically active scaffolds are based on analogues to the extracellular matrix (ECM) that have induced synthesis of tissues and organs [1]. Nanostructures are attractive for many medical applications such as tissue engineering and regeneration [2].

Nanostructures were found mechanical properties, biocompatibility and biodegradability similar to the native ECM and tended to the adhesion and proliferation of cells for repair of damaged tissues. Nanostructures of hybrid biologic materials have known as effective structures for tissue engineering [3–5]. Selection criteria for biologic materials are based on synthetic chemical chemistry, molecular weight, solubility, shape and structure, hydrophobicity, lubrication, surface energy, water absorption degradation and erosion mechanism [1] that polymers in the field of biological materials are remarkably advanced in the fabrication of tissue engineering scaffolds [6, 7]. Polymeric scaffolds are suitable for tissue engineering applications because of their high surface-to-volume ratio, biodegradability, biocompatibility, high porosity with very small pore size, good mechanical and biological properties [1].

Synthetic elastomer polymers often lack proper biocompatibility and natural polymers lack the mechanical properties needed for tissue engineering, so combining natural and synthetic materials to create composite scaffolds can be solve these challenges. The hybrid structures of proteins and synthetic polymers have the proper elasticity in tissue engineering structures [8]. PCL is an aliphatic linear biological polymer [9] and has been considered due to low tissue melting, biocompatibility, solubility, ability to maintain mechanical and physical properties, and cell and drug permeability for tissue engineering applications [10, 11]. When the force applied to PCL, it resists linear shear and pressure forces and when the force removed it returns to its original state and has good elasticity properties [10]. Therefore, PCL synthetic polymer is a potential candidate for tissue engineering applications [12]. Over the past years the combination of bioactive materials and PCL for tissue engineering and remedial medicine has received much attention and PCL scaffolds through blending with polylactic acid [13, 14], octacalcium phosphate [15], alginate [16], collagen [17], gelatin[18, 19], chitosan [20, 21] showed special characters. Gelatin is a natural biopolymer made from controlled hydrolysis of collagen that is a major component of native ECM. Gelatin has biological, biodegradability and biocompatibility properties and is commercially low cost and has many applications in pharmacology and medicine. Gelatin preserves information signals of the arginine–glycine–aspartic acid (RGD) that promotes cell adhesion, proliferation and differentiation. Therefore, gelatin can be mixed with biological polymers to fabricate tissue engineering scaffolds [21, 22]. Also, Gelatin increases the uniformity of adsorption in nanofibers, and this property of gelatin may be useful for cell adhesion uniformity [23]. The PDMS is a viscoelastic polymer, it means that at long flow times (or high temperature), it acts like a viscous liquid, similar to honey. However, at short flow times (or low temperature), it acts like an elastic solid, similar to rubber.

Viscoelasticity is a form of nonlinear elasticity that is common among noncrystalline polymers [24]. The mechanical properties of PDMS enable this polymer to conform to a diverse amount of surfaces. Since these properties are affected by a variety of factors, this unique polymer is relatively easy to tune [25, 26]. Specifically, the determination of mechanical properties can be decided before PDMS is cured. The uncured version allows the user to capitalize on myriad opportunities for achieving a desirable elastomer. Generally, the cross-linked cured version of PDMS resembles rubber in a solid form. It is widely known to be easily stretched, bent, and compressed in all the directions. Depending on the application and the field, the user can able to tune the properties based on what is demanded. PDMS network can be used as substrate to grow cells. Varying the crosslink density in the polymer network allows one to tune the mechanical properties in a range similar to living tissues. The effect of the PDMS network stiffness on the growth and behavior of cells has been studied [27].

To mimic the structure and biological function of native ECM proteins, tissue engineering scaffolds must be designed to meet the mechanical properties of the tissues and create physical, chemical, and biological properties for a good life and guidance of cells to the functional tissues via cell migration, adhesion and differentiation [28]. Electrospinning is a versatile technique as a powerful technology for the production of nanofibers with compositions, structures, and diverse properties [29]. Also, electrospinning has been considered as a versatile fiber producing method as its high potential for a variety of applications including biomedical scaffolds [30]. Depending on the type of material and application of the scaffold, the nanofibers can provide the required surface for cell activity and adjustable mechanical and biological properties [31, 32].

Composite PCL/gelatin nanofibrous scaffold by electrospinning method caused biocompatibility and enhanced cell proliferation rate [22]. Aligned nanofibers highly supported the nerve cells and improved the neurite outgrowth and cell differentiation process [33]. Also, the PCL–gelatin nanofibers crosslinked with genipin may hold a promise to be used as a substrate for the culture of muscle cells and further implantation for engineering muscle tissue [34]. Macroporous PDMS scaffold can serve as a promising material for acellular as well as cellular skin tissue dressing [35]. The advanced mechanical properties, shape memory properties and biocompatibility of these PCL–PDMS fibers would allow them to become promising candidates for tissue regeneration, and an injectable TE scaffold may be achieved based on these electrospun SMP fibers [36].

In this study, PCL/G/PDMS hybrid fibrous scaffolds with both the random and arranged fibers were fabricated using electrospinning. Then morphology, crystallinity, surface roughness and mechanical properties, and biocompatibility of the random and arranged scaffolds were studied. Growth, proliferation and morphology of the cells on scaffolds were also evaluated. Presented results indicate that the PCL/G/PDMS scaffold is a novel biocompatible scaffold, suitable for tissue engineering. This study is the first manuscript for optimization of the combination of three polymers of PCL/G/PDMS for application in tissue engineering which can replace collagen polymer in tissue engineering scaffolds. the purpose of current study is elastic scaffold design for endometrial cells, uterine tissue reconstruction and also, production of

artificial uterus in the future. Endometrial cells were cultured on the selected scaffold and yielded positive results which will be presented in the following articles.

Materials and methods

Materials

PCL (M_w = 80,000), PDMS (PDMS-diol, Mn = 2000 g/mol), gelatin powder of bovine skin were purchased from Sigma-Aldrich (St. Louis, MO) with a purity of 97%. 3-(4,5-dimethylthiazoyl-2-yl) 2,5-diphenyltetrazolium bromide (MTT) and dimethyl sulfoxide (DMSO) were purchased from Sigma-Aldrich® and trifluoroacetic acid (TFA) (C2HF3O2, 114.02 g/mol), glutaraldehyde and hematoxylin–eosin (H&E) were purchased from Merck® companies. Dulbecco's Modified Eagle Medium (DMEM), collagenase type I, fetal bovine serum (FBS) and pen-strep solution were purchased from Gibco®. Phosphate buffered saline (PBS, pH 7.4) was purchased from Inoclon®. Trypsin/ethylene diamine tetra-acetic acid (trypsin/EDTA) was purchased from Bio-Idea®. Human fibroblast Cells (Yazd human foreskin fibroblasts; YhFF#8; passage 20) were kindly gifted from the Stem Cell Biology Research Center of Yazd Reproductive Sciences Institute.

Fabrication of scaffolds

Electrospinning is a hydro-dynamic process that liquid droplet is electrified to produce a jet, which causes the fiber production by stretching and elongation. An electrical conductor is inserted between the tip of the needle and the conductor. Then the droplet becomes a cone shape structure (Taylor cone) which a charge jet is ejected. The jet first runs along a straight line then look like whipping motions. Jet converts drop into thin fibers because of bending instabilities and solidifies rapidly and produces solid fibers [29]. PCL (10 wt%), G (5 wt%) and PDMS (7 wt%) were dissolved in TFA by agitating the mixture with magnetic stirrer at 500 rpm for 2 h at room temperature (28 ± 1 °C) at various ratios 100:0:0, 90:10:0, 70:30:0, 50:50:0, 0:100:0, 90:0:10, 80:0:20, 70:0:30, 30:50:20 (optimized points in different blend ratio obtained by RSM [37, 38]), 40,40,20, 50:30:20, 60,30,10, 70:20:10, respectively. The produced fibers were coded as C10, C9G1, C7G3, C5G5, G10, C9D1, C8D2, C7D3, C3G5G2 (Optimized points in different blend ratio obtained by RSM), C4G4D2, C5G3D2, C6G3D1 and C7G2D1, respectively, based on the ratios of PCL (C), gelatin (G) and PDMS (D) in the scaffolds (Table 1) [36]. Different electrospinning parameters were tested such as applied voltage, feeding rate, needles caliber, and collector distance for the production of the smooth and beads-free composite nanofibers. The solution was infused through a 2.5 ml syringe attached to a programmable syringe pump into a 21-gage metal needle. The optimum condition was obtained after an immiscible blend of PCL/G/PDMS was obtained for electrospinning, with the feeding rate of the polymer solution at 0.1 ml h^{-1}, 22 kV of voltage and needle tip to the collector distance at 16 cm. The speeds of the collector rotation were set at 300 and 1000 rpm.

Table 1 Codes of producted fibers

Code	Polymer		
	PCL (%)	Gelatin (%)	PDMS (%)
C10	100	0	0
C9G1	90	10	0
C7G3	70	30	0
C5G5	50	50	0
G10	0	100	0
C9D1	90	0	10
C8D2	80	0	20
C7D3	70	0	30
C3G5D2	30	50	20
C4G4D2	40	40	20
C5G3D2	50	30	20
C6G3D1	60	30	10
C7G2D1	70	20	10

Characterization of composite nanofiber scaffolds

Attenuated total reflectance Fourier transform infrared spectroscopy (ATR-FTIR)

ATR-FTIR spectra of mixing percentages of three polymers were recorded using thermo nicolet ATR-FTIR. The range of wavenumbers of FTIR (Equinox 55, Bruker, Germany) was from 600 to 4000 cm^{-1}.

X-ray diffraction (XRD)

XRD patterns were recorded using X-ray diffractometer to evaluate the crystalline phase in fibers using anode Cu at 40 kV and 30 mA in 2θ the range of 5°–50°. X'Pert High Score Plus software (PANalytical®) was used for crystalline phases identification.

Scanning electron microscopy (SEM)

The morphology of composite nanofibers has been investigated with SEM (ZEISS® DSM 960A Oberkochen, Germany) with an accelerating voltage of 8 kV. The scaffolds were coated with gold before imaging. The diameter of the nanofibers was calculated from the SEM images using image analysis software (Image J, 1.41o software). The average diameter of at least 100 fibers per image (three random images per sample) was determined for each sample and reported as mean ± standard deviation (SD).

Image processing

The computation of pores on the web of nanofibers using image processing has prioritized the optimization of the image separated into two portions of fibers and pores using the *k*-means clustering algorithm. *K*-means clustering algorithm is a cluster analysis of data analytics that contributes them into predetermined clusters. The data are made up of image details, the data of each cluster being similar to the data of the other clusters. Distance is one of the criteria for clustering. The closer data are considered as one cluster. The *k*-means clustering method has been used in images threshold studies [39].

Evaluation of biodegradability of the scaffolds

The degradation behavior of the scaffolds was investigated by the immersion of scaffold samples (50 mm × 15 mm) into a Falcon tube containing 10 mL of PBS solution (pH 7.4, 37 °C). The scaffolds were dried in an oven at 37 °C until making a constant mass (W_i) before the test. At 14 and 28 days, the samples were removed from the medium, washed with distilled water, and the excess of water at the surface was withdrawn by a filter paper. After this stage, the hydrated weight (W_h) of the scaffolds was immediately evaluated to determine the water absorption. Then, the scaffolds were transferred to an oven and dried at 37 °C until stopping on a constant mass (W_f) to determine its weight loss. The medium was replaced weekly with a new fresh media. Nine samples were tested for every model [40].

$$\text{Water absorption}\,(\%) = \left(W_h - W_i\right)/W_i \times 100$$

$$\text{Weight loss}\,(\%) = \left(W_i - W_f\right)/W_i \times 100.$$

Mechanical property test

The mechanical properties of nanofiber scaffolds were determined using a tabletop uniaxial test apparatus (Instron® SANTAM-STM-20 Testing Machine). The 20-N load cell is used for tensile tests speed of 3 mm/min under ambient conditions. Scaffolds samples were cut in the dimension of $30 \times 10 \times 0.2$ mm^3. For all the samples, at least six trials were tested for each type of electrospun nanofibers.

In vitro cell culture

The fibroblasts were grown in DMEM supplemented with 10% FBS and 1% penicillin/streptomycin in 60 cm^2 tissue culture Petri dishes (TPP, Biochrom AG®, Germany) in a standard humidified incubator at 37 °C temperature and 5% carbon dioxide concentration. At a cell confluency of about 80%, the cells were washed with PBS, incubated with 0.05%/ 0.02% (v/v) trypsin/EDTA solution and pelleted by centrifugation at 200 g for 5 min. Fresh culture medium was added to the cell

pellet obtained after centrifugation, and the cell number was counted. After sterilization under UV light for 30 min, the electrospun fibers were placed in 24-well plates and were seeded with fibroblast cells at a density of 10,000 cells per well. The cells were incubated in a humidified incubator at 37 °C with 5% CO2, and the medium was changed every 3 days. Samples were harvested after 1, 3, and 7 days for H&E staining and after 5 days for SEM examination. To fix the cells on the scaffold, the medium was removed from the wells, 2.5% glutaraldehyde was added to the wells and incubated at 4 °C for 2 h.

Cell viability assay

The viability of cultured fibroblast cells on scaffolds was evaluated by MTT assay on days 1, 5 and 7. Cells were seeded at 96-well plates at a density of 1×10^4 cells per scaffold and maintained at 37 °C under 5% CO_2 concentration. 100 µL of MTT solution (0.5 mg/mL) was added to the culture medium in every well. After incubation for 4 h, the MTT solution was removed and same volume of MTT solution, isopropanol and hydrochloric acid of 0.1 normal were added to each well and were placed in the incubator for 30 min. The absorbance of samples was measured at 570–630 nm using an ELIZA reader (Expert 96, Asys Hitch®, Ec Austria).

Cell study on nanofibrous scaffold

SEM

Cell morphology on PCL/G/PDMS composite scaffolds was investigated by SEM. Fibroblast cells at a density of 10,000 cells/well were cultured on scaffolds. The cells were incubated in a humidified incubator at 37 °C with 5% CO_2 concentration and the medium was changed every 5 days. Then cells of scaffolds were fixed with 4% glutaraldehyde for 2 h at − 4 °C. After that they were rinsed with PBS and dehydrated with alcohol 70%, 96% and 100% for 5 min. The scaffolds were coated with gold and investigated by SEM.

Hematoxylin–eosin (H&E) staining

Cells were cultured on scaffolds and fixed with 2.5% glutaraldehyde 1, 3, and 7 days after culture for 2 h, then rinsed with PBS three times for 5 min. After washing, they were exposed to 100%, 96% and 70% ethanol for 5 min, respectively. Samples were stained with hematoxylin and rinsed with PBS for 5 min. The samples were treated with acid alcohol for 2 s. Samples were rinsed with PBS and stained with eosin for 2 min. Finally, they were rinsed with 70%, 96% and 100% ethanol for 5 min to dehydrate the scaffolds. H&E was performed for staining of the nuclei and cytoplasm of the cells, respectively, where the nucleus appears blue and the cytoplasm red.

Statistical analysis

The Origin 8.0 (Origin Lab Inc., USA) was used for statistical analysis. The results of the experiments were shown as mean values with standard deviation (SD). Statistical analysis was performed using one-way ANOVA, and $P < 0.05$ was considered statistically significant. Tukey's test was applied for evaluations of differences between groups.

Results and discussion

Fourier transform infrared (FTIR) spectroscopy

Figure 1 indicates the FTIR for composite scaffolds: PCL, gelatin, PCL/G, PCL/PDMS and PCL/G/PDMS. Due to asymmetric CH2 stretching, symmetric CH2 stretching, carbonyl stretching, C–O and C–C stretching, asymmetric C–O–C stretching and symmetric C–O–C stretching, several characteristic bands of PCL were observed in 2943 cm^{-1}, 2865 cm^{-1}, 1728 cm^{-1}, 1293 cm^{-1}, 1239 cm^{-1} and 1171 cm^{-1}, respectively. For N–H stretching of amide bond, C=O stretching, N–H bending and N–H out-of-plane wagging bands of gelatin were shown at 3308 cm^{-1}, 1648 cm^{-1}, 1536 cm^{-1} and 674 cm^{-1}, respectively [22]. The characteristic bands of PDMS in PCL/PDMS composite scaffold were observed in 796 cm^{-1} (Si–C stretching vibration), 1016 cm^{-1} and 1080 cm^{-1} (Si–O–Si stretching vibration), 1255 cm^{-1} and 867 cm^{-1} (rocking vibrations of Si–CH3) [41]. In PCL/G/PDMS composite scaffold, all the characteristic bands of PCL, gelatin and PDMS were observed but

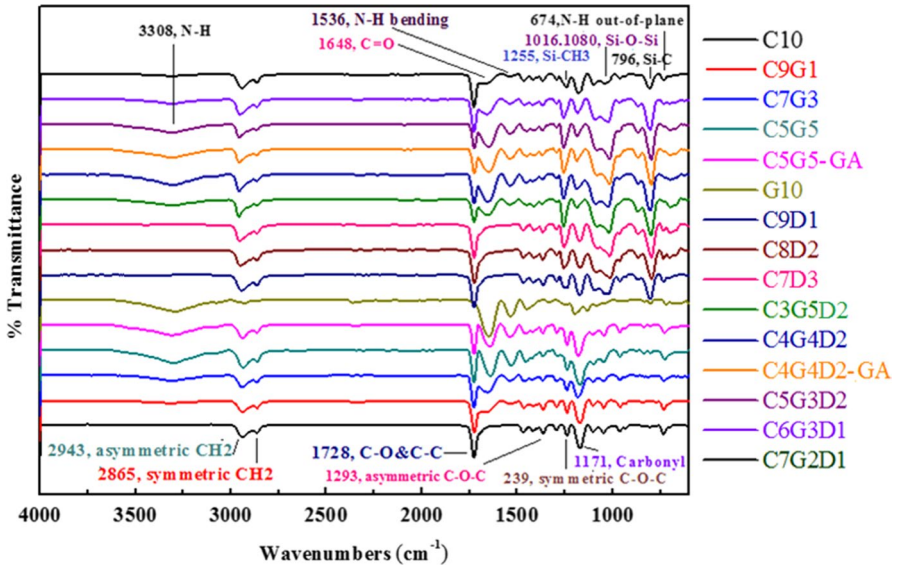

Fig. 1 ATR-FTIR spectra of PCL/G/PDMS nanofibers scaffolds with different ratios

the bands have been shifted towards the higher wavenumbers. All the peaks in the FTIR spectrum of PCL, G, PDMS were observed in the FTIR spectra of PCL/G/PDMS nanofibers. As the amount of gelatin increases, the intensity of peak for PCL and PDMS decreases, and the peak intensity of gelatin increases, and vice versa. The same absorption peaks of PCL/G/PDMS scaffolds indicate that PCL, gelatin and PDMS will not change their molecular structure in blends. The adsorption peaks of the PCL/G/PDMS scaffolds show that the PCL, G and PDMS molecular structure has not changed in the PCL/G/PDMS mixture. Also, the adsorption peaks do not change with the cross-linking of gelatin polymer with glutaraldehyde vapor in scaffolds [42]. For example, FTIR of scaffolds of C5G5 and C4G4D2 both specimens fixed with glutaraldehyde vapor (C5G5-GA and C4G4D2-GA) and without glutaraldehyde vapor (C5G5 and C4G4D2) were done and the peaks are the same for the both samples.

There is crosslinking reaction between GA and –NH2 in gelatin According to Fig. 2.

The NH2 content in gelatin decreases after crosslinking and the more GA the higher decrease degree is. The absorption peak of C=O in C5G5 and C4G4D2 moves slightly toward high wave number from 1648 to 1651 cm^{-1}. The reason may be that with addition of little GA, the hydrogen-bond interaction of intra- and inter-molecular chain weakens [44]. The absorption peak of C=O in the C5G5 and C4G4D2 moves toward low wavenumber from 1648 to 1643 cm^{-1}. The reason may be that the excess GA destroys the triple helix structure of gelatin, so hydrophilic free radicals increase and the hydrogen-bond interaction is boosted [44].

X-ray diffraction

One of the factors affecting hydrophilicity and cell behavior on the scaffolds is the crystalline and amorphous structure of their polymers.

The XRD pattern in Fig. 3 shows the sharp diffraction peak in 21.4° and low intensity peak in 23.8°, which correspond to the semi-crystalline PCL. The absence of diffraction peak in XRD pattern of gelatin indicates amorphous gelatin. XRD pattern of pure PDMS [45] and in combination with PCL and gelatin polymers exhibits an amorphous structure with a single peak of about 12°. The XRD pattern of C5G3D2 hybrid scaffold in Fig. 2 shows all the characteristic peaks of PCL with low intensity.

The reduction in the peaks in the C5G3D2 hybrid scaffold indicates a decrease in crystallinity and this crystallinity decreases and amorphous increases may be due to

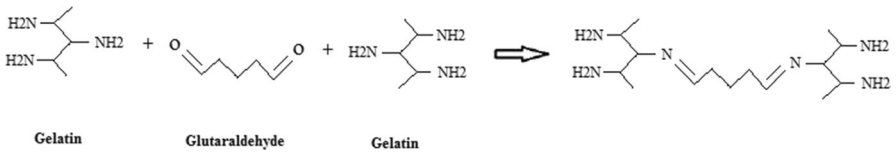

Fig. 2 Cross-linking process of gelatin nanofibers by GA [43]

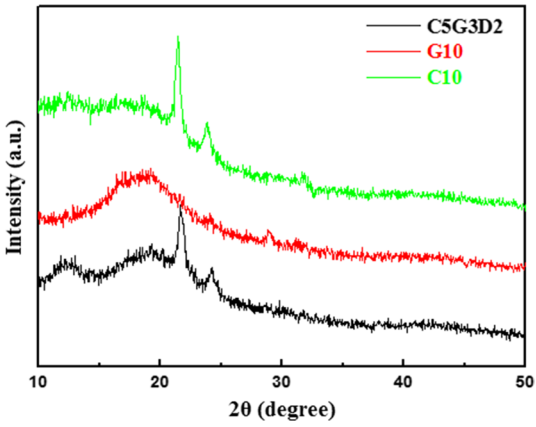

Fig. 3 X-ray diffraction patterns of C10, G10 and C5G3D2 nanofiber scaffolds

the collision of PCL molecules to gelatin and amorphous PDMS. As the amorphous structure is more suitable for cell adhesion and proliferation than the highly crystalline structure [46], so the hybrid scaffold can be a suitable substrate for cell adhesion and proliferation.

Nanofiber morphology of PCL/G/PDMS

Electrospun PCL/G/PDMS scaffolds with different weight ratios were fabricated with random and arranged morphology. The three images randomly were taken at the different points of every scaffold. One hundred diameters were measured in each image, and the mean diameters were analyzed with the origin. Figure 4 shows SEM images of different morphology for scaffolds at different PCL, G and PDMS weight ratios in random and parallel scaffolds. In these images, it is clear that with increasing the gelatin concentration, the amount of ultra-fine networks between the fibers increased. The surface of the fibers in Fig. 4 was formed consists of fibers with a diameter of 200–300 nm with a small number of thin networks (< 100 nm) between the nanofibers. SEM images consisted of thin nanofibers with diameters of < 100 nm and thick fibers with diameters of about 200–300 nm. High viscosity solutions form structures with smaller fibers between larger smooth fibers, forming the continuous web [47]. Also, gelatin is a polyelectrolyte that increases the conductivity, increases in electrical conductivity of the solution and tensile force applied to the jet, that result in the production of fine fibers [22]. Rapid phase separation of mixed polymer and solvent is the main reason for the formation of networks [47]. Networks increase the surface area, cell adhesion and expansion. As shown in Fig. 5, collector speed increases during the electrospinning process decreases network formation. Also, with increase in gelatin percentage of the hybrid polymers, nanofiber networks increase and the fibers approach from the arranged state to the random state. Network is rarely found in gelatin (G10) scaffolds. Nanofibers without gelatin polymer in their structure, due to the lack of networks have significant makeup and fibers are almost aligned. The viscosity and conductivity of polymer solutions of PCL, gelatin, C5G5 and C3G5D2 at a final concentration of 12 wt% in the solvent

system are measured. Pristine PCL solution showed a viscosity of 61.2 cP, whereas the conductivity was 13.1 µS. Conversely, gelatin solution showed the lowest viscosity (19.8 cP) and highest conductivity (398.9 µS), C5G5 and C3G5D2 solutions showed a viscosity of 32.4 cP and 31.5 cP, and the conductivity was 51.6 µS and 49.8 µS, respectively, whereas the composite solutions showed a gelatin concentration dependant decrease in viscosity and increase in conductivity.

The average diameters of hybrid nanofiber and networks with different percentages of PCL/G/PDMS areshown in Fig. 4 ($P < 0.05$).

The diameter of the nanofibers of random (300 rpm) compared with the diameter of the arranged nanofibers (1000 rpm) increase in all percentages but the diameter of the networks does not change. As the collector speed increases, the tension between the feeding syringe tip and the collector increases, this reduces the diameter of the fibers. With cross-linking of gelatin polymer with glutaraldehyde vapor, the fibers become denser and as a result of this shrinkage the fibers form a crimped structure that mimics the collagen-like structure [42, 48].

Figure 6 demonstrates the orientation distribution of nanofibers extracted from Polar alignment software. False color orientation map of nanofibers extracted from the SEM image. The radial axis represents the main number of pixels of orientation for the nanofibers. The black line in the center in Fig. 6a shows the average orientation of the nanofibers. As Fig. 6a shows the color orientation of each pixel of nanofibers corresponds to the alignment of nanofibers in the color wheel. S_{2D}, as a function of frame size describe the decay of the orientation order parameter. The variance of the orientation distribution is captured by the orientational order parameter S_{2D}, sometimes referred to as Herman's Orientation Factor. Mathematically, S_{2D} is defined as:

$$S_{2D} = 2\left(\mathrm{COS}^2\theta_n\right) - 1 \tag{1}$$

where θ_n is the angle between an individual fiber pixel and the image's overall director, n, which is chosen as the average orientation of the population. In the context of this analysis, S_{2D} varies between 0 and 1; the expected value of $\cos^2\theta$ for a population of random angles θ is 0.5, yielding an S_{2D} of 0 invariant to the selection of the director, and a perfectly ordered population generates an $\langle\cos^2\theta_n\rangle$ of 1, yielding an S_{2D} of 1. The director is plotted in each Orientation Distribution as a centered black line segment, as in Fig. 6b [49].

Nanofiber porosity of PCL/G/PDMS composite

Due to the development of nanofibers in different industries, it is important to know the morphology of nanofibers structures to understand the distribution of fiber dimensions and pores. Tissue engineering scaffolds must have a porous structure for cell infiltration and proliferation within the scaffold as well as to ensure the adequate exchange of gas and nutrients for tissue regeneration. Nanofibers provide highly porous assemblies and networks create a large surface area for cell proliferation and migratio. Networks are useful in cell growth and proliferation on the scaffolds. Also,

Fig. 4 SEM images of electrospun PCL/G/PDMS hybrid scaffolds of random and arrangement with different ratios. By adding gelatin to PCL and PDMS polymers, the diameter of the nanofibers decreases and the number of networks increases ▶

as the nanofibers arrangement increases in the scaffolds the porosity decreases. So, cell penetration may be reduced on the arranged scaffolds.

Threshold capture is a simple and effective technique for image segmentation. Many threshold methods have been developed so far. One of the methods that have been considered in recent years is the *k*-means clustering method. Calculation of pores has been done on the nanoweb and nanofibers using image processing and achieving optimum image separated into two portions of fibers and pores by the *k*-means clustering algorithm [39]. The steps of calculation of porosity of nanofibers in the image processing are as follows: (1) Reading of the image, (2) Image filtering to remove noise, (3) Extract image data (4) Use *k*-means function for image clustering, (5) Separate clusters. Because the best image is black and white, the sum of the black images in every image is porosity (Fig. 7).

One of the causes of pore formation in the scaffold may be rapid evaporation of TFA and rapid solidification of PCL/G/PDMS during the process of nanofibers production. As shown in Fig. 8, the porosity decreases with increases in gelatin content due to increases in the networks formation, but the presence of polymers of PCL and PDMS with the production of thicker nanofibers cause a gap in the scaffolds. Also, increases in the porosity decreases the aligned nanofibers. This change in porosity in aligned and random nanofibers is most evident in scaffolds without gelatin.

Biodegradability of the PCL/G/PDMS scaffolds

One of the properties of polymers used in tissue engineering is the synchronization of time appropriate of destruction with the needed time to reconstruct or treat [50]. Polymers of PCL and gelatin are biodegradable polymers [51]. Although PDMS is a non-biodegradable polymer (and biocompatible) but PCL/PDMS copolymer is used as a biodegradable option in reconstruction medicine. For biodegradable PCL, as time passes with increased porosity, the cells penetrate and at the same time non-biodegradable PDMS with mechanical support provides the basis for cell migration and attachment [36]. The images shown in Fig. 9 for the gelatin nanofibers and networks display loss of visibility of scaffolds after 14 days and for the scaffolds with lesser percentage of PCL/PDMS, they exhibit smaller surface erosion and a slower linear degradation due to slow hydrolysis of the PCL molecules. At 28 days, the networks were completely hydrolyzed, and nanofibers showed more considerable degradation relative to 14 days. At the SEM images of nanofibers scaffolds with PCL/G/PDMS ratios were taken 14 and 28 days after degradation, nanofiber surface becomes rough by a uniform degradation process that results in faster penetration of water into the nanofibers. As mentioned in the XRD explanation by adding gelatin and PDMS to PCL polymer, the crystallization of PCL decreases so the degradation rate of the PCL/G/PDMS nanofibers scaffolds increases. The process of uniform

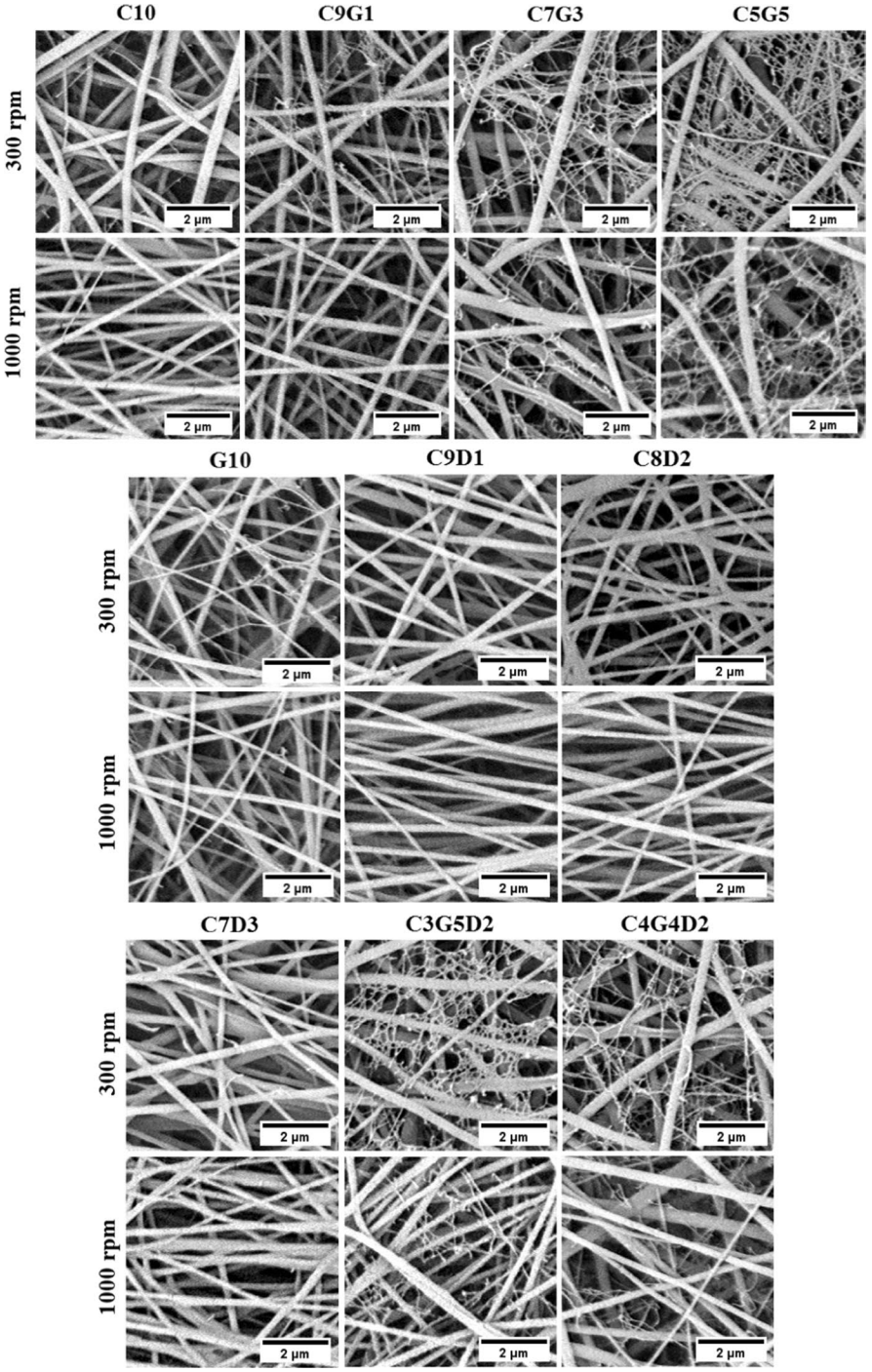
C10
C9G1
C7G3
C5G5
300 rpm
1000 rpm
2 µm
G10
C9D1
C8D2
C7D3
C3G5D2
C4G4D2

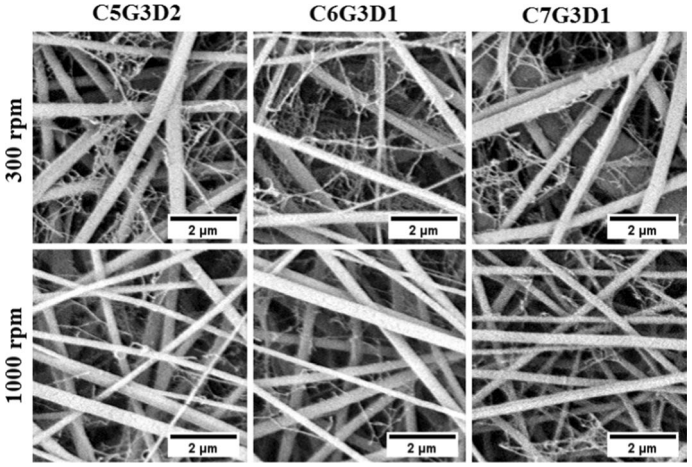

Fig. 4 (continued)

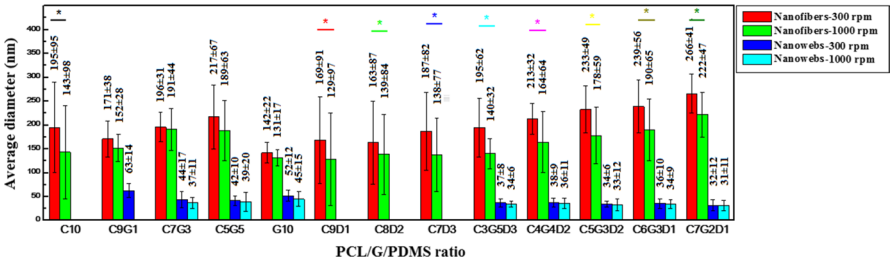

Fig. 5 Variations in the diameter of nanofibers and networks with different PCL/G/PDMS ratios by collector speed at 300 rpm and 1000 rpm. Results are expressed as mean ± SD (*$P < 0.05$)

degradation of PCL/G/PDMS nanofibers indicates the intermingling of PCL, gelatin and PDMS polymer chains.

Mass loss of PCL/G/PDMS nanofiber scaffolds after 14 and 28 days is presented in Fig. 10. The mass loss of PCL/G/PDMS is much higher than that of PCL and PDMS alone because of the degradation of gelatin [50].

After being PCL degradation, the tensile strength of the scaffolds and after gelatin degradation, elongation are enough to form new tissues [52]. The optimum tensile stregth value for formation of new tissue is listed in Table 3. The results have shown that degradation occurs in scaffolds with PCL, gelatin and PDMS.

Mechanical properties of PCL/ G/ PDMS scaffolds

Porous scaffolds for tissue regeneration must be strong enough to withstand forces during surgery and tissue growth. The PCL [48] and PDMS have good mechanical properties [35, 38, 53]. The mechanical properties of scaffolds made by

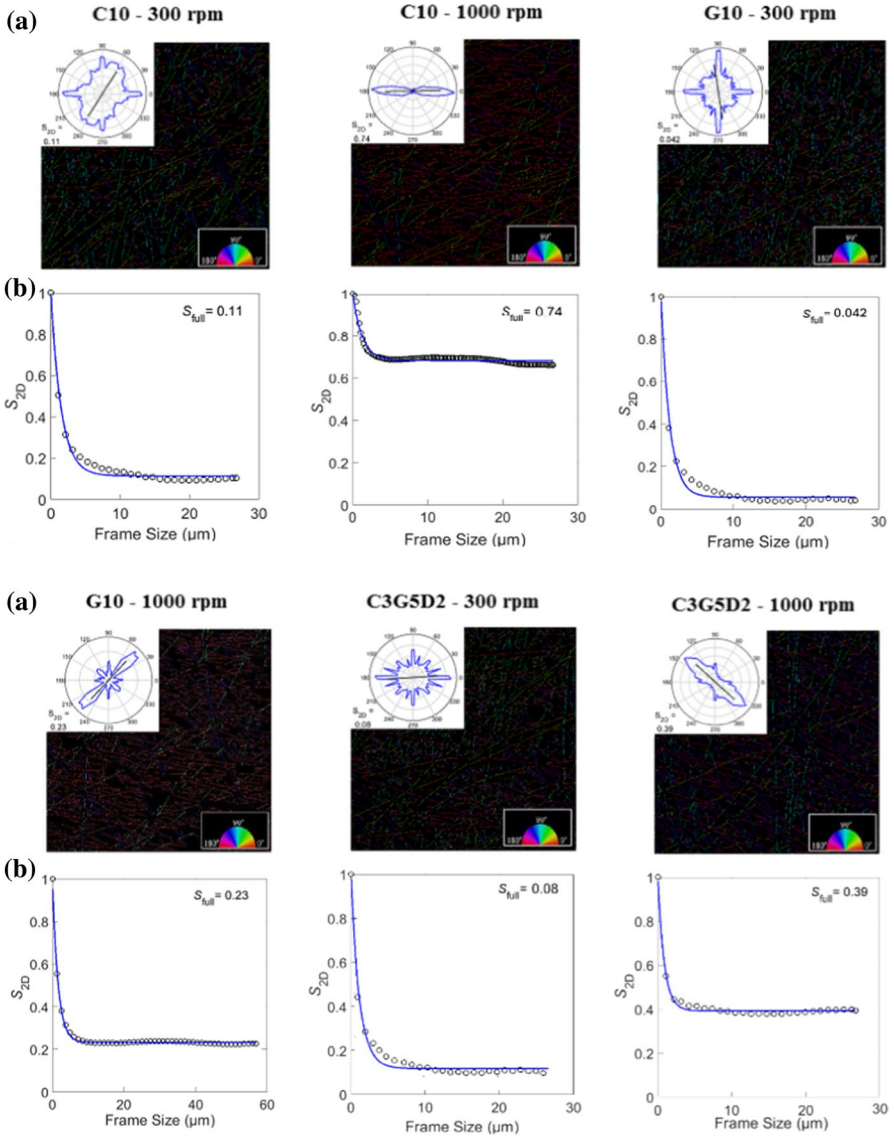

Fig. 6 Orientation distribution of nanofibers extracted from Polar alignment software. **a** False color orientation map of nanofibers extracted from the SEM image. The radial axis represents the number of pixels of orientation of nanofibers. The black line in the center shows the average orientation of the nanofibers. The color orientation of each pixel of nanofibers corresponds to the alignment of nanofibers in the color wheel. **b** The decay of the orientation order parameter, S_{2D}, is a function of frame size. The full-frame value of S_{2D} is written in the images

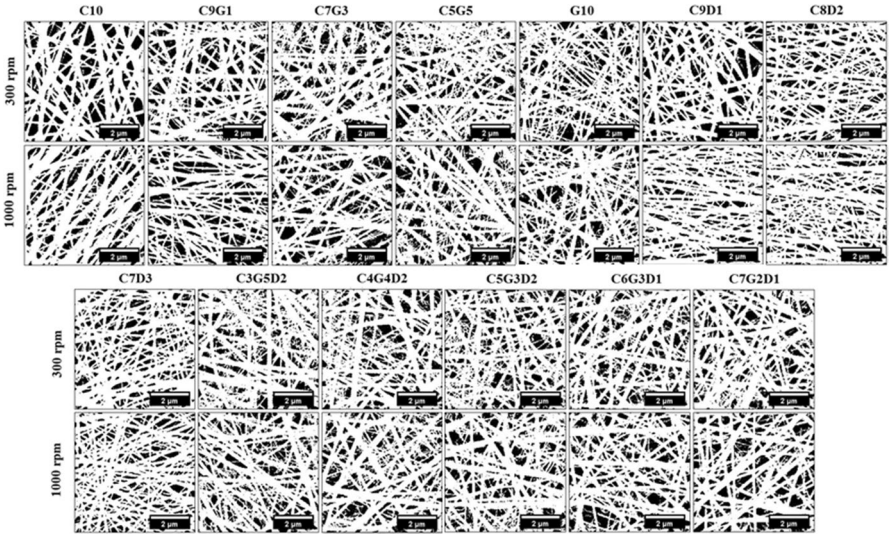

Fig. 7 Nanofiber threshold of SEM images with the *k*-means algorithm

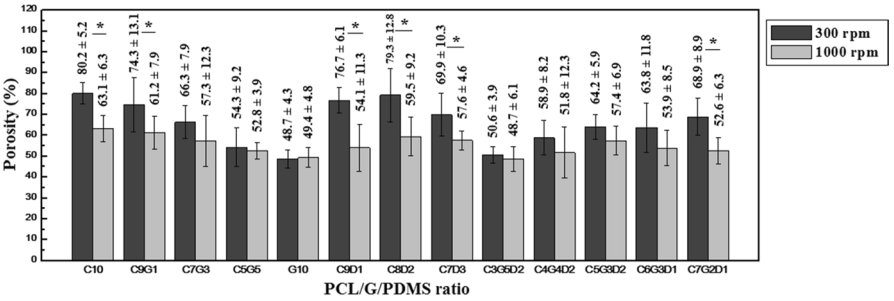

Fig. 8 Porosity graphs of nanofibers and network formation with different PCL/G/PDMS ratios by collector speed at 300 rpm and 1000 rpm. Results are expressed as mean ± SD (*$P < 0.05$)

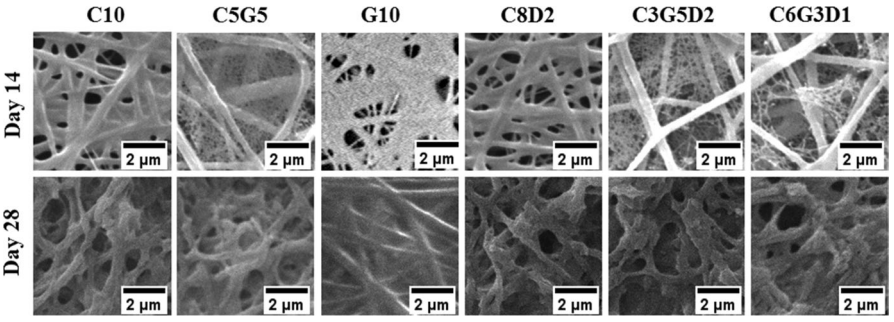

Fig. 9 SEM images of electrospun PCL/G/PDMS hybrid scaffolds with different ratio after 14 and 28 days of biodegradation

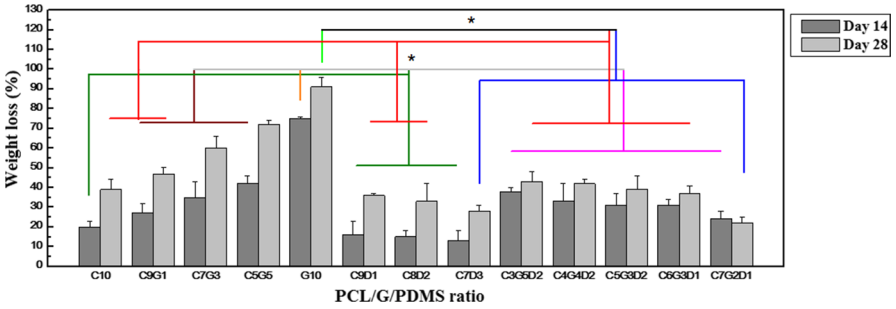

Fig. 10 Biodegradable graphs of nanofibers and networks with PCL/G/PDMS different ratios. Results are expressed as mean ± SD (*$P < 0.05$)

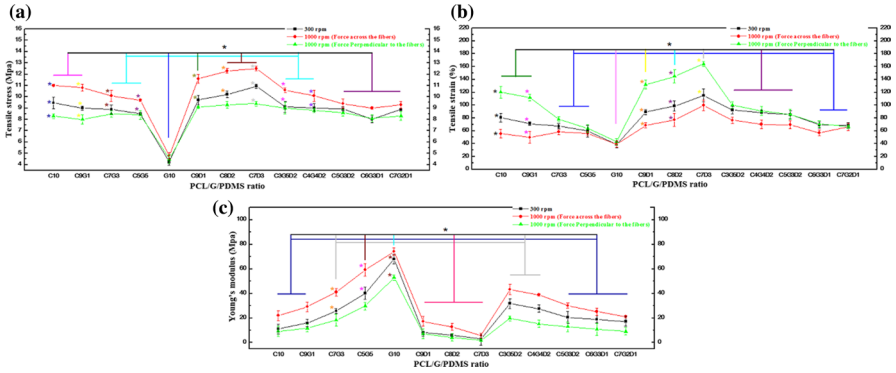

Fig. 11 Mechanical properties of the electrospun PCL/G/PDMS nanofiber: **a** tensile strengths, **b** strain at break and **c** Young's modules. PCL/G/PDMS ratio and nanofibers arrangement were important factors in determining the nanofibers mechanical properties. Results are expressed as mean ± SD (*$P < 0.05$)

electrospinning depend on the chemical composition and morphology of the nanofibers [36]. Figure 11 displays ultimate tensile strength, strain at break and Young's modulus of scaffolds with PCL/G/PDMS various ratios. With increasing the PDMS ratio in the blend polymers, the tensile strengths and strain at break increase and the Young's modulus decrease. Also, tensile strengths, strain at break and Young's modules curves show that increasing PCL ratio and, especially PDMS ratio increases the elastic properties of the scaffolds [36]. In contrast, with increasing the gelatin ratio in the blend polymers, the tensile strengths and strain at break, decrease and the Young's modulus increases. Also, porosity significantly affect the mechanical properties of the scaffolds [35]. Therefore, the decrease in the mechanical properties of the scaffolds with increase in gelatin can be due to both the poor mechanical properties of the gelatin and also due to the reduction of porosity of the scaffolds [33] (Fig. 11, Table 2).

As Fig. 11a and Table 2 show, the arranged nanofibers strength increases in the fiber direction and decreases in the perpendicular direction to the fibers. Also,

Table 2 Applications of PCL/G/PDMS scaffolds based on morphology and mechanical properties

	Tensile stress (Mpa)			Tensile strain (%)			Young's modules (Mpa)		
PCL/G/PDMS nanofibers	300 rpm	1000 rpm (Forse across the fibers)	1000 rpm (Forse perpendicular to the fibers	300 rpm	1000 rpm (Forse across the fibers)	1000 rpm (Forse perpendicular to the fibers	300 rpm	1000 rpm (Forse across the fibers)	1000 rpm (Forse perpendicular to the fibers
C10	9.46	11	8.3	80.5	55.6	120.3	11	22	9.2
C9G1	9.01	10.8	8	71.1	49.8	111.7	15.9	29.2	11.7
C7G3	8.88	10.1	8.5	67.2	58.2	77.9	25.7	41.1	18.2
C5G5	8.51	9.7	8.4	59.6	55.7	63.8	40.1	59.2	29.7
G10	4.24	4.8	4.5	38.4	39.2	43.2	67.9	74.2	52.9
C9D1	9.73	11.6	9.1	89.2	68.4	132.1	8.2	17.2	7.1
C8D2	10.21	12.3	9.3	98.7	77.1	144.8	5.9	12.8	4.2
C7D3	10.93	12.5	9.4	115.1	99.8	164.2	2.9	5.8	1.9
C3G5D2	9.12	10.6	9	92.3	76.5	100.2	31.8	43.2	19.7
C4G4D2	9.01	10.1	8.8	88.4	70.1	91.1	27.6	38.9	15.2
C5G3D2	8.92	9.4	8.6	85.2	69.4	85.7	20.5	30.1	12.9
C6G3D1	8.01	9	8.1	69.3	56.8	70.6	18.9	25.2	10.8
C7G2D1	8.88	9.3	8.3	68.4	66.1	66.3	17.2	21.1	9.1

Fig. 11b and Table 2 show that the elongation decreases in the fiber direction and increases in the perpendicular direction to the fibers relative to the random nanofibers [33]. Therefore, based on the strength, elongation and morphology of elastic tissues, scaffolds with different percentages of three polymers of PCL, gelatin and PDMS can be used.

Cell viability and proliferation on the PCL/G/PDMS scaffolds

In order to evaluate non-toxicity of scaffolds and fibroblasts interaction with PCL/G/PDMS hybrid scaffolds, the MTT assay was performed on scaffolds containing cells on 1, 5 and 7 days. Glass coverslips without any electrospun scaffold were used as control.

At the first day, the cell compatibility with scaffold had confirmed at 570 adsorption and with the gelatin and PDMS percentage increasing to PCL have increased cell proliferation on scaffolds in random and aligned nanofibers. The cell proliferation increasing percentage on the scaffolds with gelatin increasing more than the PDMS increasing (Fig. 12) due to gelatin excellent cell adhesion and proliferation properties [29, 54]. After 7 days, the highest YhFF#8 cells proliferation occurred on the scaffolds.

At days 1, 5 and 7 cell growth and proliferation according to percentage of cell survival versus compound concentration (absorbance at 570 nm) on the random scaffolds were more significant than the aligned scaffolds, and this may be due to the reduced porosity and hydrophilicity of the aligned scaffolds. The MTT assay and solution absorbance at 570 nm for evaluation of cell compatibility with scaffolds and comparison with the control sample showed that the nanohybrid scaffolds were not toxic. Also, scaffolds containing gelatin and PDMS cell growth and proliferation were better than control ($P < 0.05$).

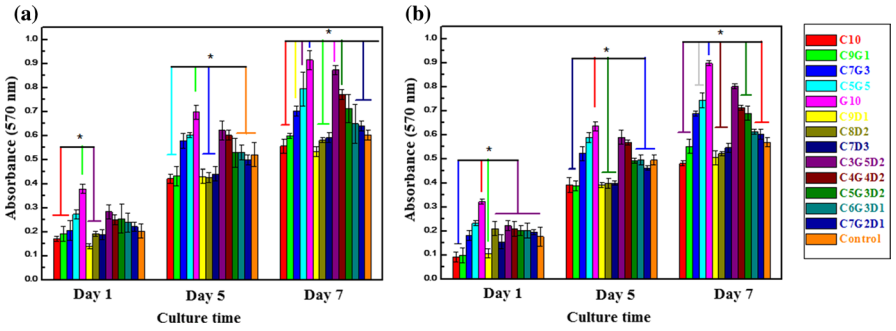

Fig. 12 Cell viability and proliferation on PCL/G/PDMS scaffolds with different ratio and control sample (glass coverslips). **a** Random nanofibers (300 rpm), **b** aligned nanofibers (1000 rpm). Increased viability and proliferation of cells correlate well with increase in gelatin percentage. Results are expressed as mean ± SD (*$P < 0.05$)

Cell attachment, spreading and morphology on the PCL/G/PDMS scaffolds

Attachment, proliferation and morphology of cells on random and aligned scaffolds were studied with H&E staining after 1, 3 and 7 days and SEM images on day 5. Glass coverslips without any electrospun scaffold were used as control. As shown in Figs. 13 and 14, the morphology of cells on random and aligned scaffolds is different and cells reacted to random and aligned architecture of scaffolds. Cell attachment

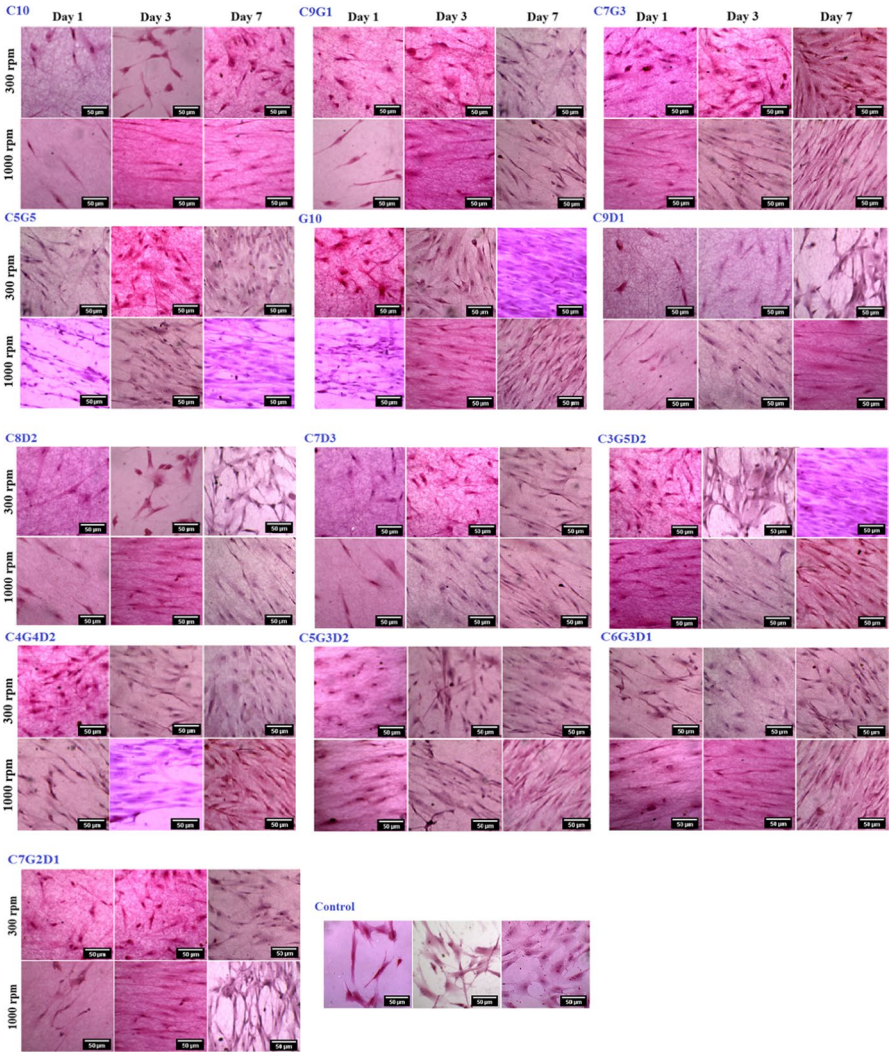

Fig. 13 H&E staining micrographs of fibroblasts (YhFF#8) cultured on PCL/G/PDMS scaffolds with different ratio and control sample (glass coverslips) after 1, 3 and 7 days. In both of random (300 rpm) and aligned nanofiber (1000 rpm), the highest proliferation of cells was with gelatin and PDMS percentage increasing to PCL. Scale bar 50 µm

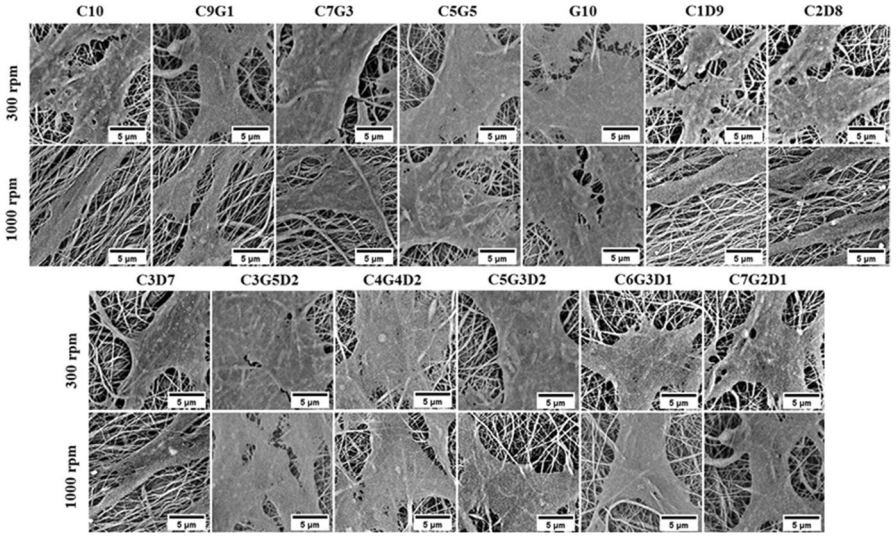

Fig. 14 SEM micrographs of fibroblasts cultured on PCL/G/PDMS scaffolds with various ratios

and proliferation among the scaffolds visualized using SEM, H&E staining. Microscopic data showed that fibroblasts attached and spread over the entire scaffolds surface (Figs. 13, 14). The cells on random scaffolds widely attached to the entire surface of the scaffolds, spread and had a flat morphology. In contrary, the cells on aligned scaffolds attached along the fibers and were assembled on the surface in the direction of the nanofibers, creating a uniform linear pattern and showed spindle shape morphology.

After 7 days, an extensive group of cells on the scaffolds proliferated and attached (Fig. 13). Increased cell adhesion and proliferation with increasing gelatin content is due to the protein content and fast degradability of gelatin polymer to form scaffold structure [55] and the large surface area of the networks in these scaffolds.

As indicated in SEM micrographs (Fig. 14), fibroblasts attached and generated an extensive network of cells after 5 days on the hybrid scaffolds.

With the scaffolds increasing in gelatin content, the nanofibers exit the aligned configuration toward the random nanofibers, which may be due to the presence of network formation in the scaffolds (Fig. 14).

These results showed that PCL/G/PDMS hybrid scaffold promoted the fibroblast cell adhesion and proliferation and the morphology of the PCL/G/PDMS scaffolds make changes in the morphology of the cells.

Table 3 Applications of PCL/G/PDMS scaffolds based on morphology and mechanical properties

Tissue type	Morphology of the scaffold	Stress at failure (Mpa)	Strain at failure (%)	Modulus (Mpa)	Suggested scaffold	References
Peripheral nerve	Aligned	6.78 ± 0.57	61 ± 2	15.87 ± 2.21	C7G3 C5G3D2	Chiono et al. [56]
Uterus	Random	0.1–2.06	19–43	0.023–0.04	C3G5D2, C4G4D2 C5G3D2 C6G3D1	Manoogian et al. [57] Omari et al. [58] Yen and Jaffe's [59]
Bladder	Random	0.5–2.6 (mean stress, 0.9 ± 0.1 MPa)	-	1–4.1 (mean stiffness, 1.9 ± 0.2 MPa)	C7G3, C5G5 C3G5D2 C4G4D2	Martins et al. [60] Chantereau et al. [61] Atala [62]
Trachea Cartilage	Aligned Random	0.58	-	3.33 ± 0.49	C7G3 C6G3D1, C7G2D1	Trabelsi et al. [63] Crowley et al. [64]
Trachea: smooth muscle (longitudinal direction)	Aligned	0.001	34.16	0.000154	C7G3 C5G3D2 C6G3D1 C7G2D1	Trabelsi et al. [63]
Trachea: smooth muscle (transversal direction)	Aligned	0.001 stress mean of transversal and longitudinal direction	13.89	0.000347	C7G3 C5G3D2 C6G3D1 C7G2D1	Trabelsi et al. [63]
Aortic heart valves	Random Aligned	-	68.85	0.156 ± 0.025	C3G5D2, C4G4D2 C5G3D2	Liao et al. [65] Vesely [66]
Vagina	Random	2.4 ± 0.53	19.0 ± 5	27.0 ± 11.5	C7G3, C5G5 C3G5D2, C4G4D2	Feola et al. [67] Silveira et al. [68]
umbilical artery	Aligned	1.8	14	10	C9G1, C5G3D2 C6G3D1, C7G2D1	Karimi et al. [69]

Table 3 (continued)

Tissue type	Morphology of the scaffold	Stress at failure (Mpa)	Strain at failure (%)	Modulus (Mpa)	Suggested scaffold	References
Vascular: saphenous vein (longitudinal direction)	Aligned	5.38 ± 0.6	1.32 ± 0.04	5.7	C9G1 C5G3D2 C6G3D1 C7G2D1	Hamedani et al. [70] Sankaran et al. [71] Zorlutuna et al. [72]
Vascular: saphenous vein (transversal direction)	Aligned	2.61 ± 0.67	1.55 ± 0		C9G1 C5G3D2 C6G3D1 C7G2D1	Hamedani et al. [70]
umbilical vein(longitudinal direction)	Aligned	1.65 ± 0.11	1.33 ± 0.04	1.55	C9G1, C5G3D2 C6G3D2 C7G2D1	Hamedani et al. [70]
umbilical vein (transversal direction)	Aligned	0.97 ± 0.19	1.9 ± 0.16	-	C9G1, C5G3D2 C6G3D2 C7G2D1	Hamedani et al. [70]
Liver	Random	0.094	10.6–24.6	0.52–1.78	C9G1, C7G3 C5G3D2, C6G3D1	Mattei et al. [73] Yoon No et al. [74]
Back skin	Random	21.6 ± 8.4	54 ± 17	83.3 ± 34.9	C9G1 C6G3D1, C7G2D1	Annaidh et al. [75] Alexey et al. [76]
Abdomen skin	Random	1–24	17–207	2.9–54.0	C7G3, C5G5 C4G4D2, C5G3D2	Jansen and Rottier [77]
Thorax Skin	Random	2–15	-	18.8	C9G1, C4G4D2 C5G3D2, C6G3D1, C7G2D1	Dunn and sliver [78]
Forehead, arm skin	Random	5.7–12.6	27–59	19.5–87.1	C7G3	Jacquemoud et al. [79]

Applications of PCL/G/PDMS scaffolds with various ratios

According to literature review, applications of PCL/G/PDMS scaffolds with various ratios based on cell morphology and mechanical properties according to cell attachment and proliferation are shown in Table 3.

Conclusion

In this study, the hybrid fibrous scaffolds of PCL, gelatin and PDMS with two various types of fiber arrangement were fabricated with different mass ratio by electrospinning. Physicochemical properties of electrospun PCL/G/PDMS hybrid nanofibers were investigated for their influences on cell growth, proliferation and morphology and their selection for potential scaffolds for elastic tissue engineering. The results have shown that the mechanical and structural properties of the PCL/G/PDMS scaffolds are among the major factors for the cell growth and proliferation on the scaffolds. By addition of gelatin to nanofibers due to its protein nature and fast degradability, producing the large surface area of networks in scaffolds, amorphous structure of gelatin increases cell adhesion and proliferation on hybrid nanofibers and decreases nanofibers alignment and porosity. Adding the PDMS polymer to PCL/G improves the mechanical properties, especially the elasticity of the scaffolds, also it slightly improves in cell adhesion to the scaffolds due to the PDMS amorphous structure. Biocompatibility and non-toxicity of PCL/G/PDMS nano-hybrid scaffolds in contact with fibroblasts have been confirmed by MTT assay. The morphology of cells on random and aligned scaffolds is different and cells reacted to the both type of scaffolds. The cells on random scaffolds widely attached to the entire surface of the scaffolds and spread well and had a flat morphology. In contrast, the cells on aligned scaffolds attached along the fibers and were assembled on the surface in the direction of the nanofibers, creating a uniform linear pattern and converted into spindle shape morphology.

Due to the mechanical properties, morphology, biodegradability and biocompatibility of the scaffolds, these scaffolds may be suitable for both random (e.g., for liver or skin tissues) and aligned (e.g., for nerve) tissue engineering applications, including elastic organs like uterus, blood vessels, bladder, trachea, heart valves, vein, vagina, and others.

Acknowledgements This work was supported by Iran national science foundation (INSF; Project No. 97014466), Yazd University Research Council and Yazd Reproductive Sciences Institute for their financial support**.** We are grateful to Dr. Behrouz Aflatoonian and Fatemeh Sadeghian-Nodoushan for their cooperation and technical support.

Declarations

Conflict of interest The authors declare that they have no conflict of interest in the data presented in this manuscript.

References

1. Dhandayuthapani B, Yoshida Y, Maekawa T, Kumar DS (2011) Polymeric scaffolds in tissue engineering application: a review. Int J Polym Sci 2011:1–19
2. Habibi N, Kamaly N, Memic A, Shafiee H (2016) Self-assembled peptide-based nanostructures: smart nanomaterials toward targeted drug delivery. Nano Today 11:41–60
3. Wang P, Zhao L, Liu J, Weir MD, Zhou X, Xu HHK (2014) Bone tissue engineering via nanostructured calcium phosphate biomaterials and stem cells. Bone Res 2:14017
4. Armentano I, Bitinis N, Fortunati E, Mattioli S, Rescignano N, Verdejo R, Lopez-Manchado MA, Kenny JM (2013) Multifunctional nanostructured PLA materials for packaging and tissue engineering. Prog Polym Sci 38:1720–1747
5. Li X, Wang L, Fan Y, Feng Q, Cui F-Z, Watari FJ (2013) Nanostructured scaffolds for bone tissue engineering. Biomed Mater Res A 101A:2424–2435
6. Piskin E (1995) Biodegradable polymers as biomaterials. J Biomater Sci Polym Ed 6:775–795
7. Ji Y, Ghosh K, Zheng Shu X, Li B, Sokolov JC, Prestwich GD, Clark RAF, Rafailovich MH (2006) Electrospun three-dimensional hyaluronic acid nanofibrous scaffolds. Biomaterials 27:3782–3792
8. Coenen AMJ, Bernaerts KV, Harings JAW, Jockenhoevel S, Ghazanfari S (2018) Elastic materials for tissue engineering applications: natural, synthetic, and hybrid polymers. Acta Biomater 79:60–82
9. Hajiali F, Tajbakhsh S, Shojaei A (2018) Fabrication and properties of polycaprolactone composites containing calcium phosphate-based ceramics and bioactive glasses in bone tissue engineering: a review. Polym Rev 58:164–207
10. Hench LL (1991) Bioceramics: from concept to clinic. J Am Ceram Soc 74:1487–1510
11. CSIRO Molecular Science, Bag 10, Clayton South MDC, Vic 3169, Australia and Gunatillake P (2003) Eur Cell Mater 5:1–16
12. Bhat S, Chen C, Day DA (2013) Effects of a polycaprolactone (PCL) tissue scaffold in *Rattus norvegicus* on blood flow. MRS Proc 1498:27–31
13. Zhao P, Gu H, Mi H, Rao C, Fu J, Turng L (2018) Fabrication of scaffolds in tissue engineering: a review. Front Mech Eng 13:107–119
14. Jammalamadaka U, Tappa K (2018) Recent advances in biomaterials for 3D printing and tissue engineering. J Funct Biomater 9:22
15. Heydari Z, Mohebbi-Kalhori D, Afarani MS (2017) Engineered electrospun polycaprolactone (PCL)/octacalcium phosphate (OCP) scaffold for bone tissue engineering. Mater Sci Eng C 81:127–132
16. Kundu J, Shim J-H, Jang J, Kim S-W, Cho D-W (2015) An additive manufacturing-based PCL-alginate-chondrocyte bioprinted scaffold for cartilage tissue engineering. J Tissue Eng Regen Med 9:1286–1297
17. Zhang YZ, Venugopal J, Huang Z-M, Lim CT (2005) Characterization of the surface biocompatibility of the electrospun PCL-collagen nanofibers using fibroblasts. Biomacromolecules 6:2583–2589
18. Rajzer I, Rom M, Menaszek E, Pasierb P (2015) Conductive PANI patterns on electrospun PCL/gelatin scaffolds modified with bioactive particles for bone tissue engineering. Mater Lett 138:60–63
19. Chong EJ, Phan TT, Lim IJ, Zhang YZ, Bay BH, Ramakrishna S, Lim CT (2007) Evaluation of electrospun PCL/gelatin nanofibrous scaffold for wound healing and layered dermal reconstitution. Acta Biomater 3:321–330
20. Jing X, Mi H-Y, Wang X-C, Peng X-F, Turng L-S (2015) Shish-kebab-structured poly(ε-caprolactone) nanofibers hierarchically decorated with chitosan–poly(ε-caprolactone) copolymers for bone tissue engineering. ACS Appl Mater Interfaces 7:6955–6965
21. Gomes SR, Rodrigues G, Martins GG, Roberto MA, Mafra M, Henriques CMR, Silva JC (2015) In vitro and in vivo evaluation of electrospun nanofibers of PCL, chitosan and gelatin: a comparative study. Mater Sci Eng C 46:348–358
22. Gautam S, Dinda AK, Mishra NC (2013) Fabrication and characterization of PCL/gelatin composite nanofibrous scaffold for tissue engineering applications by electrospinning method. Mater Sci Eng C 33:1228–1235
23. Mansoori S, Davarnejad R, Matsuura T (2020) Membranes based on non-synthetic (natural) polymers for wastewater treatment. Polym Test 84:106381
24 Courtney TH (2013) Mechanical behavior of materials. McGraw Hill Education (India), New Delhi
25. Rogers JA, Nuzzo RG (2005) Recent progress in soft lithography. Mater Today 8:50–56

26. McDonald JC, Duffy DC, Anderson JR, Chiu DT, Wu H, Schueller OJA, Whitesides GM (2000) Fabrication of microfluidic systems in poly(dimethylsiloxane). Electrophoresis 21:27–40
27. Wang Zh, Volinsky AA, Gallant N (2011) Polydimethylsiloxane mechanical properties measured by macroscopic compression and nanoindentation techniques. University of South Florida Scholar Commons
28. Nalwa HS (ed) (2003) Handbook of photochemistry and photobiology. American Scientific Publishers, Stevenson Ranch, CA
29. Xue J, Wu T, Dai Y, Xia Y (2019) Electrospinning and electrospun nanofibers: methods, materials, and applications. Chem Rev 119:5298–5415
30. Sagitha P, Reshmi CR, Sundaran SP, Sujith A (2018) Recent advances in post-modification strategies of polymeric electrospun membranes. Eur Polym 105:227–249
31. Pham QP, Sharma U, Mikos AG (2006) Electrospinning of polymeric nanofibers for tissue engineering applications: a review. Tissue Eng 12:1197–1211
32. Hasan A, Memic A, Annabi N, Hossain M, Paul A, Dokmeci MR, Dehghani F, Khademhosseini A (2014) Electrospun scaffolds for tissue engineering of vascular grafts. Acta Biomater 10:11–25
33. Ghasemi-Mobarakeh L, Prabhakaran MP, Morshed M, Nasr-Esfahani MH, Ramakrishna S (2008) Electrospun poly(3-caprolactone)/gelatin nanofibrous scaffolds for nerve tissue engineering. Biomaterials 29:4532–4539
34. Kim MS, Jun I, Shin YM, Jang W, Kim SI, Shin H (2010) The development of genipin-crosslinked poly(caprolactone) (PCL)/gelatin nanofibers for tissue engineering applications. Macromol Biosci 10:91–100
35. Varshney N, Sahi AK, Vajanthri KY, Poddar S, Balavigneswaran CK, Prabhakar A, Rao V, Mahto SK (2019) Culturing melanocytes and fibroblasts within three-dimensional macroporous PDMS scaffolds: towards skin dressing material. Cytotechnology 71:287–303
36. Kai D, Prabhakaran MP, Chan BQY, Liow SS, Ramakrishna S, Xu F, Loh XJ (2016) Elastic poly(ε-caprolactone)-polydimethylsiloxane copolymer fibers with shape memory effect for bone tissue engineering. Biomed Mater 11:015007
37. Dehghan M, Khajeh-Mehrizi M, Nikukar H (2020) Modeling and optimizing a polycaprolactone/gelatin/polydimethylsiloxane nanofiber scaffold for tissue engineering: using response surface methodology. J Text Inst 112:482–493
38. Dehghan M, Nikukar H, Khajeh-Mehrizi M (2020) Optimizing the physical parameters of polycaprolactone–gelatin–polydimethylsiloxane composite nanofibr scaffold for tissue engineering application. J Ind Text. https://doi.org/10.1177/1528083720960156
39. Dehghan N, Tavanaie MA, Payvandy P (2015) Morphology study of nanofibers produced by extraction from polymer blend fibers using image processing. Korean J Chem Eng 32:1928–1937
40. Ifkovits JL, Burdick JA (2007) Review: photopolymerizable and degradable biomaterials for tissue engineering applications. Tissue Eng 13:2369–2385
41. Pereira RF, Carvalho A, Gil MH, Mendes A, Bártolo PJ (2013) Influence of Aloe vera on water absorption and enzymatic in vitro degradation of alginate hydrogel films. Carbohydr Polym 98:311–320
42. Lu W, Ma M, Xu H, Zhang B, Cao X, Guo Y (2015) Gelatin nanofibers prepared by spiral-electrospinning and cross-linked by vapor and liquid-phase glutaraldehyde. Mater Lett 140:1–4
43. Morsy R, Hosny M, Reisha F, Elnimr T (2017) Developing and physicochemical evaluation of cross-linked electrospun gelatin-glycerol nanofibrous membranes for medical applications. J Mol Struct 1135:222–227
44. Zhan J, Morsi Y, El-Hamshary H, Al-Deyab SS, Mo X (2016) In vitro evaluation of electrospun gelatin-glutaraldehyde nanofibers. Front Mater Sci 10:90–100
45. Sun K, Xie P, Wang Z, Su T, Shao Q, Ryu JE, Zhang X, Guo J, Shankar A, Li J, Fan R, Cao D, Guo Z (2017) Flexible polydimethylsiloxane/multi-walled carbon nanotubes membranous metacomposites with negative permittivity. Polymer 125:50–57
46. Cui H, Sinko PJ (2012) The role of crystallinity on differential attachment/proliferation of osteoblasts and fibroblasts on poly (caprolactone-co-glycolide) polymeric surfaces. Front Mater Sci 6:47–59
47. Heikkilä P, Harlin A (2008) Parameter study of electrospinning of polyamide-6. Eur Polym J 44:3067–3079
48. Monroy DAP, Bravo JMC, Mercado IES, Gómez LJV (2018). In tissue regeneration, HA. hay E-S Kaoud, Ed. InTech

49. Persson NE, McBride MA, Grover MA, Reichmanis E (2017) Automated analysis of orientational order in images of fibrillar materials. Chem Mater 29:3–14
50. Xue J, He M, Liu H, Niu Y, Crawford A, Coates PD, Chen D, Shi R, Zhang L (2014) Drug loaded homogeneous electrospun PCL/gelatin hybrid nanofiber structures for anti-infective tissue regeneration membranes. Biomaterials 35:9395–9405
51. Kai D, Liow SS, Loh XJ (2014) Biodegradable polymers for electrospinning: towards biomedical applications. Mater Sci Eng C 45:659–670
52. Xue J, He M, Liang Y, Crawford A, Coates P, Chen D, Shi R, Zhang L (2014) Fabrication and evaluation of electrospun PCL–gelatin micro-/nanofiber membranes for anti-infective GTR implants. J Mater Chem B 2:6867–6877
53. Mohanty S, Alm M, Hemmingsen M, Dolatshahi-Pirouz A, Trifol J, Thomsen P, Dufva M, Wolff A, Emnéus J (2016) 3D printed silicone-hydrogel scaffold with enhanced physicochemical properties. Biomacromolecules 17:1321–1329
54. Liu Y, Chan-Park MB (2010) A biomimetic hydrogel based on methacrylated dextran-graft-lysine and gelatin for 3D smooth muscle cell culture. Biomaterials 31:1158–1170
55. Beachley V, Wen X (2009) Fabrication of nanofiber reinforced protein structures for tissue engineering. Mater Sci Eng C 29:2448–2453
56. Chiono V, Tonda-Turo C (2015) Trends in the design of nerve guidance channels in peripheral nerve tissue engineering. Prog Neurobiol 131:87–104
57. Manoogian SJ, Bisplinghoff JA, Kemper AR, Duma SM (2012) Dynamic material properties of the pregnant human uterus. J Biomech 45:1724–1727
58. Omari EA, Varghese T, Kliewer MA, Harter J, Hartenbach EM (2015) Dynamic and quasi-static mechanical testing for characterization of the viscoelastic properties of human uterine tissue. J Biomech 48:1730–1736
59. Strauss JF, Barbieri RL, Eds, Yen & Jaffe's (2019) Reproductive endocrinology: physiology, pathophysiology, and clinical management. Elsevier, Philadelphia, PA
60. Martins PALS, Filho ALS, Fonseca AMRM, Santos A, Santos L, Mascarenhas T, Natal Jorge RM, Ferreira AJM (2011) Uniaxial mechanical behavior of the human female bladder. Int Urogynecol J 22:991–995
61. Chantereau P, Brieu M, Kammal M, Farthmann J, Gabriel B, Cosson M (2014) Mechanical properties of pelvic soft tissue of young women and impact of aging. Int Urogynecol J 25:1547–1553
62. Atala A (2011) Tissue engineering of human bladder. Br Med Bull 97:81–104
63. Trabelsi O, Del Palomar AP, López-villalobos JL, Ginel A, Doblaré M (2010) Experimental characterization and constitutive modeling of the mechanical behavior of the human trachea. Med Eng Phys 32:76–82
64. Crowley C, Birchall M, Seifalian AM (2015) Trachea transplantation: from laboratory to patient: trachea transplantation. J Tissue Eng Regen Med 9:357–367
65. Liao J, Joyce EM, Sacks MS (2008) Effects of decellularization on the mechanical and structural properties of the porcine aortic valve leaflet. Biomaterials 29:1065–1074
66. Vesely I (2005) Heart valve tissue engineering. Circ Res 978:743–755
67. Feola A, Abramowitch S, Jones K, Stein S, Moalli P (2010) Parity negatively impacts vaginal mechanical properties and collagen structure in rhesus macaques. Am J Obstet Gynecol 203:595.e1-595.e8
68. Brandão R, da Silveira SD, Milhem Haddad J, Katalin I, de Jármy-Di BZ, Nastri F, Goncalves-Markos Kawabata M, Silva Carramão SD, Alves Rodrigues C, ChadaBaracat C, Pedro Flores Auge A (2015) Multicenter, randomized trial comparing native vaginal tissue repair and synthetic mesh repair for genital prolapse surgical treatment. Int Urogynecol J 26:335–342
69. Karimi A, Navidbakhsh M, Alizadeh M, Shojaei A (2014) A comparative study on the mechanical properties of the umbilical vein and umbilical artery under uniaxial loading. Artery Res 8:51–56
70. AlhosseiniHamedani B, Navidbakhsh M, AhmadiTafti H (2012) Comparison between mechanical properties of human saphenous vein and umbilical vein. Biomed Eng 11:59
71. Sankaran KK, Vasanthan KS, Krishnan UM, Sethuraman S (2014) Development and evaluation of axially aligned nanofibres for blood vessel tissue engineering: small-diameter aligned nanofibrous vascular graft. J Tissue Eng Regen Med 8:640–651
72. Zorlutuna P, Elsheikh A, Hasirci V (2009) Nanopatterning of collagen scaffolds improve the mechanical properties of tissue engineered vascular grafts. Biomacromolecules 10:814–821
73. Mattei G, Ahluwalia A (2016) Sample, testing and analysis variables affecting liver mechanical properties: a review. Acta Biomater 45:60–71

74. Yoon No D, Lee K-H, Lee J, Lee S-H (2015) 3D liver models on a microplatform: well-defined culture, engineering of liver tissue and liver-on-a-chip. Lab Chip 15:3822–3837
75. NíAnnaidh A, Bruyère K, Destrade M, Gilchrist MD, Otténio M (2012) Characterization of the anisotropic mechanical properties of excised human skin. J Mech Behav Biomed Mater 5:139–148
76. Bashkatov AN, Genina EA, Tuchin VV (2011) Optical properties of skin, subcutaneous, and muscle tissues: a review. J Innov Opt Health Sci 4:9–38
77. Jansen LH, Rottier PB (1958) Some mechanical properties of human abdominal skin measured on excised strips. Dermatology 117:65–83
78. Dunn MG, Silver FH (1983) Viscoelastic behavior of human connective tissues: relative contribution of viscous and elastic components. Connect Tissue Res 12:59–70
79. Jacquemoud C, Bruyere-Garnier K, Coret M (2007) Methodology to determine failure characteristics of planar soft tissues using a dynamic tensile test. J Biomech 40:468–475

Authors and Affiliations

Mahdieh Dehghan[1,2] · Habib Nikukar[2,3] · Mohammad Khajeh Mehrizi[1]

[1] Textile Engineering Department, Faculty of Engineering, Yazd University, Yazd, Iran

[2] Medical Nanotechnology and Tissue Engineering Research Center, Yazd Reproductive Sciences Institute, Shahid Sadoughi University of Medical Sciences, Yazd, Iran

[3] Department of Advanced Medical Sciences and Technologies, School of Paramedicine, Shahid Sadoughi University of Medical Sciences, Yazd, Iran